CBX7 is a tumor suppressor in mice and humans

Floriana Forzati, … , Monica Fedele, Alfredo Fusco

Research Article   Oncology

The *CBX7* gene encodes a polycomb group protein that is known to be downregulated in many types of human cancers, although the role of this protein in carcinogenesis remains unclear. To shed light on this issue, we generated mice null for *Cbx7*. Mouse embryonic fibroblasts derived from these mice had a higher growth rate and reduced susceptibility to senescence compared with their WT counterparts. This was associated with upregulated expression of multiple cell cycle components, including cyclin E, which is known to play a key role in lung carcinogenesis in humans. Adult *Cbx7*-KO mice developed liver and lung adenomas and carcinomas. In in vivo and in vitro experiments, we demonstrated that CBX7 bound to the *CCNE1* promoter in a complex that included HDAC2 and negatively regulated *CCNE1* expression. Finally, we found that the lack of CBX7 protein expression in human lung carcinomas correlated with *CCNE1* overexpression. These data suggest that CBX7 is a tumor suppressor and that its loss plays a key role in the pathogenesis of cancer.

Find the latest version:

https://jci.me/58620/pdf

CBX7 is a tumor suppressor in mice and humans

Floriana Forzati,[1] Antonella Federico,[1,2] Pierlorenzo Pallante,[1,2] Adele Abbate,[1] Francesco Esposito,[1]
Umberto Malapelle,[2,3] Romina Sepe,[1] Giuseppe Palma,[1,4] Giancarlo Troncone,[2,3]
Marzia Scarfò,[5] Claudio Arra,[4] Monica Fedele,[1] and Alfredo Fusco[1,2]

[1]Istituto di Endocrinologia ed Oncologia Sperimentale del CNR, Dipartimento di Biologia e Patologia Cellulare e Molecolare, Facoltà di Medicina e Chirurgia, Università di Napoli "Federico II," Naples, Italy. [2]CEINGE-Centro Biotecnologie Avanzate, Naples, Italy. [3]Dipartimento di Anatomia Patologica e Citopatologia, Facoltà di Medicina e Chirurgia, Università di Napoli "Federico II", Naples, Italy. [4]Istituto Nazionale dei Tumori, Fondazione Pascale, Naples, Italy.
[5]IRGS-Biogem, Ariano Irpino, Italy.

The *CBX7* gene encodes a polycomb group protein that is known to be downregulated in many types of human cancers, although the role of this protein in carcinogenesis remains unclear. To shed light on this issue, we generated mice null for *Cbx7*. Mouse embryonic fibroblasts derived from these mice had a higher growth rate and reduced susceptibility to senescence compared with their WT counterparts. This was associated with upregulated expression of multiple cell cycle components, including cyclin E, which is known to play a key role in lung carcinogenesis in humans. Adult *Cbx7*-KO mice developed liver and lung adenomas and carcinomas. In in vivo and in vitro experiments, we demonstrated that CBX7 bound to the *CCNE1* promoter in a complex that included HDAC2 and negatively regulated *CCNE1* expression. Finally, we found that the lack of CBX7 protein expression in human lung carcinomas correlated with *CCNE1* overexpression. These data suggest that CBX7 is a tumor suppressor and that its loss plays a key role in the pathogenesis of cancer.

Introduction

CBX7 is a chromobox family protein and a member of the polycomb repressive complex 1 (PRC1) that, together with PRC2, maintains developmental regulatory genes in a silenced state (1–3). Mouse Cbx7 associates with facultative heterochromatin and with the inactive X chromosome, thereby implicating the CBX7 protein in the repression of gene transcription (4, 5). We previously reported that the *CBX7* gene is drastically downregulated in thyroid carcinomas and that its expression progressively decreases with malignant grade and neoplastic stage (6). Indeed, CBX7 protein levels decrease in an increasing percentage of cases from benign adenomas to papillary, follicular, and anaplastic thyroid carcinomas. Moreover, restoration of CBX7 expression in thyroid cancer cells reduces growth rate, with retention of cells in the G1 phase, which suggests that CBX7 is critical for the regulation of transformed thyroid cell proliferation (6).

The correlation of the loss of CBX7 with a highly malignant phenotype and a consequent poor prognosis appears to be a general event in oncology. In fact, loss of CBX7 expression has been recently shown to be also associated with increasing malignancy grade in bladder (7), pancreatic (8), breast (9), gastric (10), and colon (11) carcinoma, whereas maintenance of CBX7 expression generally correlates with a longer survival (11). These data suggest that the loss of CBX7 expression may be strictly correlated with the acquisition of invasiveness accompanied by the loss of epithelial features and the acquisition of a mesenchymal phenotype, a process known as the epithelial-mesenchymal transition (EMT). Consistent with this hypothesis, we recently demonstrated that CBX7 is able to positively regulate *CDH1* expression, which plays a critical role in maintaining normal epithelial cell morphology, by interacting with histone deacetylase 2 (HDAC2) and inhibiting its activity on the *CDH1* promoter (12). The positive correlation between CBX7 and E-cadherin expression has been shown in thyroid (12) and pancreatic (8) carcinomas.

It is noteworthy that, in seeming contrast with our previous data, *CBX7* has been described as an oncogene (13). Indeed, it cooperates with c-Myc to produce highly aggressive B cell lymphomas and can initiate T cell lymphomagenesis (3). Moreover, CBX7 extends the lifespan of a wide range of normal human cells and immortalizes mouse fibroblasts by downregulating expression of the *Ink4a* (also known as *Arf*) locus (13, 14), and its ablation, by shRNA treatment, inhibits growth of normal cells through induction of the *Ink4a* locus (14). Therefore, in an attempt to better understand the role of CBX7 in the regulation of cell growth and its potential involvement in carcinogenesis, as well as to define its physiologic function in vivo, we examined the consequences of disrupting the *Cbx7* gene in mice.

Here, we report that both heterozygous and homozygous *Cbx7*-KO mice (*Cbx7*^{+/–} and *Cbx7*^{–/–}, respectively) showed increased susceptibility to developing benign and malignant liver and lung neoplasias. Consistently, mouse embryonic fibroblasts (MEFs) derived from the *Cbx7*-KO mice had a higher growth rate and delayed senescence compared with their WT counterparts. The ability of CBX7 to counteract activation of *CCNE1* expression by the HMGA proteins probably accounts for some phenotypic features of the *Cbx7*-KO mice. We also found an inverse correlation between CBX7 and cyclin E expression in human lung carcinomas, which indicates that the loss of *CBX7* gene expression plays a relevant role in lung carcinogenesis.

Results

Generation of Cbx7-KO mice. We used gene targeting techniques in ES cells to generate a null mutation at the murine *Cbx7* genomic locus. The targeting vector was designed to replace exons 5 and 6 of the mouse *Cbx7* gene with a neomycin cassette (Figure 1A). Exons 5 and 6 code for the C-terminal region of the protein, including the Pc-box domain required for its functions. Progeny of chimeric animals were identified by Southern blot analysis of *Eco*RI-digested tail DNA (Figure 1B), and matings were established to produce mice heterozygous or homozygous for
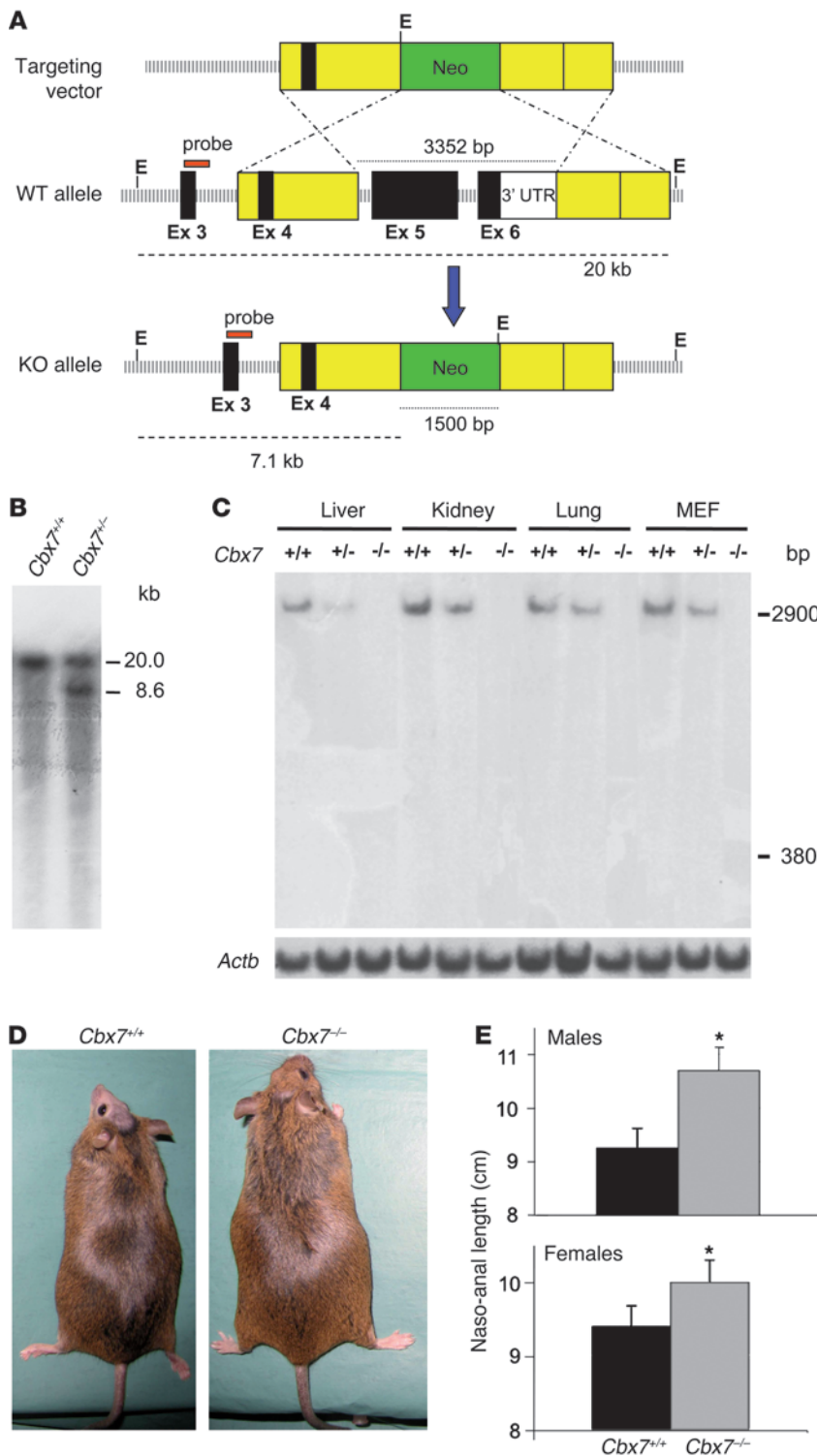
Figure 1
Generation of *Cbx7*-KO mice. (**A**) Endogenous WT allele, targeting vector, and resulting KO allele. E, *Eco*RI; Neo, neomycin; Ex, exon. (**B**) Southern blot of representative *Cbx7*^{+/+} and *Cbx7*^{+/-} ES cell clones. (**C**) Northern blot analysis of total RNA from kidneys, lungs and MEFs of *Cbx7*^{+/+}, *Cbx7*^{+/-}, and *Cbx7*^{-/-} mice. The lengths of the WT *Cbx7* transcript (2,900 bp) and the predicted truncated form after homologous recombination with the *Cbx7*-KO construct (380 bp) are shown. The absence of a 380-bp signal in both *Cbx7*^{+/-} and *Cbx7*^{-/-} mice is likely the result of instability of the short transcript. *Actb* expression analysis of the same blot is shown as control of RNA loaded. (**D**) Gross appearance of a representative 1-year-old *Cbx7*^{-/-} mouse and a sex-matched *Cbx7*^{+/+} sibling. (**E**) Naso-anal length of cohorts of 20 mice, males or females, was measured at 12 months of age. Values are mean ± SD. *$P < 0.05$.

to the potential transcript of exons 1–4 of the *Cbx7* gene that are not disrupted by the targeting construct. Moreover, Western blot performed using antibodies able to recognize the 5′ region of the CBX7 protein did not show the expression product of the potential truncated transcript (Supplemental Figure 1; supplemental material available online with this article; doi:10.1172/JCI58620DS1). It is likely that this short messenger is degraded and does not code for any protein.

Heterozygote matings yielded *Cbx7*^{+/+}, *Cbx7*^{+/-}, and *Cbx7*^{-/-} offspring at roughly the expected Mendelian ratio, indicative of no marked embryonic lethality. Interestingly, *Cbx7*-KO mice showed a significant increase in naso-anal body length: 70% of females and 46% of males showed average increases of 6.5% ($P = 0.041$) and 16% ($P = 0.044$), respectively, compared with their WT counterparts (Figure 1, D and E).

Cbx7^{-/-} *MEFs grow faster and senesce later than do their Cbx7*^{+/+} *counterparts*. To investigate the role of CBX7 in cellular proliferation, we analyzed the growth rate and cell cycle distribution of MEFs from *Cbx7*^{+/+}, *Cbx7*^{+/-}, and *Cbx7*^{-/-} embryos at 12.5 dpc. As shown in Figure 2A, growth rate was significantly higher in *Cbx7*^{-/-} MEFs than in *Cbx7*^{+/+} controls, and intermediate in *Cbx7*^{+/-} MEFs. To assess whether the higher growth rate of *Cbx7*^{-/-} MEFs was caused by deranged progression through the phases of the cell cycle, we examined asynchronously growing MEFs by flow cytometry. The number of *Cbx7*^{-/-} MEFs was lower in G$_1$ and higher in S phase of the cell cycle compared with *Cbx7*^{+/+} MEFs (Figure 2B). Consistently, the *Cbx7*^{-/-} MEFs transiently transfected with a Myc-Hys–tagged *Cbx7* expression vector showed a decreased number of cells in the S phase and an increased cell population in the G$_1$ phase of the cell cycle compared with backbone vector–transfected *Cbx7*^{-/-} MEFs (Figure 2C).

the *Cbx7*-null allele. To verify the absence of *Cbx7* expression in *Cbx7*^{-/-} mice, total RNA from the kidney, liver, lung, and MEFs of WT and *Cbx7*-KO mice was assayed by Northern blot. As expected, *Cbx7*^{-/-} mutants did not express the *Cbx7* transcript that was present in tissues from WT mice, whereas *Cbx7*^{+/-} mutants expressed an intermediate amount of *Cbx7* mRNA (Figure 1C). Northern blot did not show any band of 380 bp, corresponding
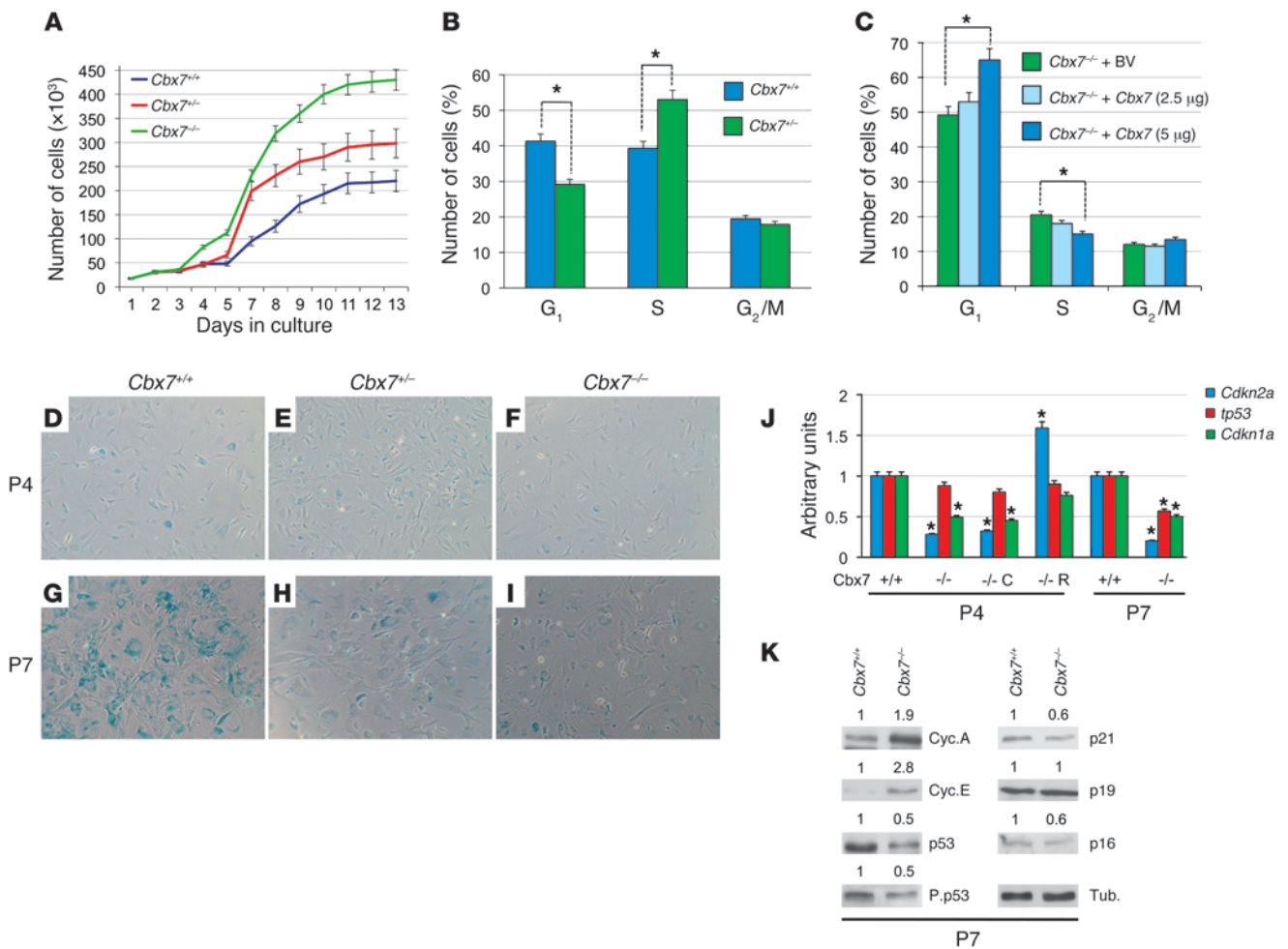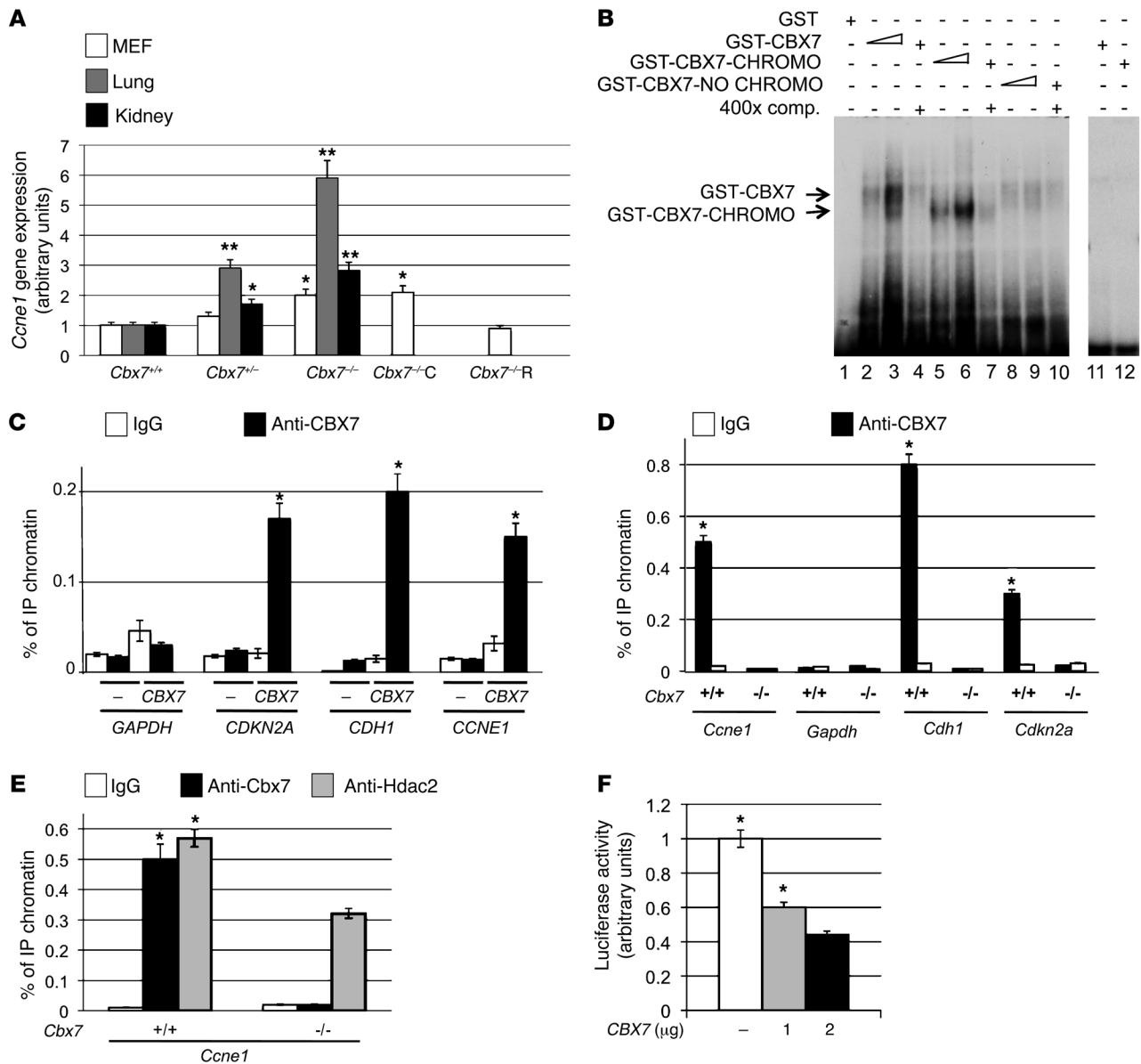
Figure 2
Growth alterations in *Cbx7*-KO MEFs. (**A**) MEFs were prepared from *Cbx7*+/+, *Cbx7*+/–, and *Cbx7*–/– embryos at 12.5 dpc. At culture passage 4, they were plated and counted daily for 13 days to extrapolate growth curves. Shown are mean ± SEM of 3 different cell clones (each originating from a different embryo) for each genotype. (**B** and **C**) Propidium iodide flow cytometry of asynchronous growing WT and *Cbx7*-KO MEFs. (**B**) Percent cells in each phase of the cell cycle (mean ± SEM). *$P < 0.05$. (**C**) FACS analysis of *Cbx7*–/– MEFs transiently transfected with different amounts of a *Cbx7* expression vector or the backbone vector (BV). (**D–I**) Light microscopy of representative *Cbx7*+/+ (**D** and **G**), *Cbx7*+/– (**E** and **H**), and *Cbx7*–/– (**F** and **I**) MEF clones stained for β-galactosidase activity at culture passages 4 (P4; **D–F**) and 7 (**G–I**). (**J**) Expression of cell cycle inhibitors *Cdkn2a*, *tp53*, and *Cdkn1a* in representative MEFs from each genotype was determined by qRT-PCR at culture passages 4 and 7. *$P < 0.05$. Passage 4 *Cbx7*–/– MEFs transiently transfected with the backbone vector (C) or whose *Cbx7* expression had been restored (R) are also shown. (**K**) Expression of cell cycle and senescence regulators in representative MEFs from each genotype was determined by Western blot at culture passage 7. Normalized protein levels, evaluated by densitometric analysis, are indicated above immunoblots.

We next examined the susceptibility to senescence of the MEFs at different culture passages by measuring senescence-associated β-gal (SA–β-gal) activity. Starting from culture passage 7, SA–β-gal activity was present in WT MEFs, as evidenced by the presence of green cells (Figure 2G). Conversely, SA–β-gal activity was absent from most of the *Cbx7*-KO counterparts (Figure 2, H and I). These findings suggest a role of CBX7 in the induction of cellular senescence. Senescent MEFs express elevated levels of p21 and p16 consequent to replication and culture stress (15). These 2 genes may cooperate to inhibit Rb phosphorylation and maintain growth arrest in an irreversible state. Therefore, we evaluated mRNA and protein levels of p16, p53, and p21 in WT and *Cbx7*-KO MEFs by quantitative RT-PCR (qRT-PCR) and Western blot analysis. The mRNA and

protein expression levels of p16 (starting from passage 4) and of p53 and p21 (at passage 7) were significantly lower in *Cbx7*-KO than in WT MEFs (Figure 2K). Consistently, the levels of S15-phosphorylated p53 paralleled those of p21, and both cyclin A and cyclin E were upregulated in *Cbx7*–/– versus *Cbx7*+/+ MEFs (Figure 2K). Moreover, *Cbx7*–/– MEFs in which *Cbx7* expression had been restored — but not those transfected with empty vector — showed *Cdkn2a* and *trp53* transcript levels comparable to those observed in WT MEFs, and significantly increased *Cdkn1a* levels compared with WT (Figure 2J).

Interestingly, MEFs isolated from 2 transgenic mouse lines overexpressing *Cbx7* under the transcriptional control of a cytomegalovirus promoter (Supplemental Figure 2A) showed a behavior opposite to that of *Cbx7*-KO MEFs: a lower proliferation rate
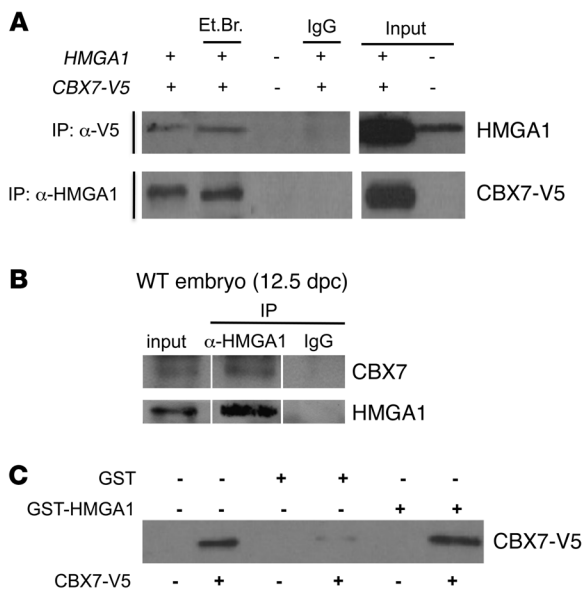
Figure 3

CBX7-dependent regulation of *Ccne1* expression. (**A**) qRT-PCR on MEFs and tissues from WT and *Cbx7*-KO mice, including *Cbx7*$^{-/-}$ MEFs transiently transfected with the backbone vector (*Cbx7*$^{-/-}$C) or whose *Cbx7* expression had been restored (*Cbx7*$^{-/-}$R), to detect *Ccne1* expression. (**B**) EMSA performed with a radiolabeled *CCNE1* promoter oligonucleotide incubated with 5 and 20 ng of the recombinant GST-CBX7 (lanes 2 and 3), GST-CBX7-CHROMO (lanes 5 and 6), or GST-CBX7-NOCHROMO (lanes 8 and 9) proteins. Where indicated, a 400-fold molar excess of unlabeled *CCNE1* promoter oligonucleotide was added (lanes 4, 7, and 10). Further negative controls were obtained by incubating the recombinant proteins with a radiolabeled *GAPDH* promoter oligonucleotide (lanes 11 and 12). (**C**–**E**) Results of ChIP assays. *CDKN2A* and *CDH1* promoters were used as positive controls, whereas *GAPDH* promoter and nonspecific IgG instead of anti-CBX7 were used as negative controls. (**C**) ChIP assay on HEK 293 cells transfected with *CBX7*-expressing or empty vector for binding of CBX7 to the *CCNE1* promoter. (**D**) ChIP assay on MEFs for binding of endogenous Cbx7 to the *Ccne1* promoter. (**E**) ChIP assay on MEFs for binding of endogenous Cbx7 and Hdac2 to the *Ccne1* promoter. (**F**) *CCNE1* promoter–driven luciferase activity, relative to activation of empty vector–transfected cells, in HEK 293 cells. Where indicated, 1 and 2 μg of *CBX7* was cotransfected with the cyclin E–luc plasmid. *$P < 0.05$; **$P < 0.01$.

(Supplemental Figure 2B) that was Cbx7 dose dependent, with a reduced cell population in the S phase of the cell cycle (data not shown). Consistently, decreased *Ccne1*, *Ccna2*, and *Ccnb1* expression was observed in MEFs of both transgenic mouse lines compared with the WT MEFs (Supplemental Figure 2A).

CBX7 binds and negatively regulates the CCNE1 promoter. In an attempt to understand the mechanism by which CBX7 negatively regulates the G$_1$/S transition, we focused on the *CCNE1* gene for various reasons: (a) it is crucial for the G$_1$/S transition during the mammalian cell cycle (16); (b) its promoter contains an E-box that

Figure 4
CBX7 interacts with HMGA1b. (**A**) HEK 293 cells were transfected with both *CBX7-V5* and *HMGA1b* expression plasmids. Cellular lysates were prepared, and equal amounts of proteins were subjected to IP with anti–CBX7-V5, anti-HMGA1, or nonspecific IgG, as indicated. The immunocomplexes were immunoblotted with reciprocal antibodies. As a positive control, 50 μg of transfected cell lysates were separated on the polyacrylamide gel as input. Et.Br., ethidium bromide. (**B**) Tissue lysates were prepared from WT embryos, and equal amounts of proteins were subjected to IP with anti-HMGA1 antibodies or nonspecific IgG. The immunocomplexes were immunoblotted with anti-CBX7 antibodies, for detection of the co-IP, or with anti-HMGA1 antibodies, for the IP control. As a positive control, 100 μg tissue lysates were used as input. Lanes were run on the same gel but were noncontiguous (white lines). (**C**) GST-HMGA1b or GST proteins immobilized on glutathione beads were used to bind CBX7-V5 from HEK 293 cells. The filter was probed with the anti–CBX7-V5 antibody.

is also present in the region recognized by CBX7 on the *CDH1* promoter (12); (c) it is positively regulated by E2F3, whose activity is negatively modulated by chromatin-regulating and -remodeling proteins, including HDAC and PcG proteins (17, 18); and (d) its overexpression is frequently associated with lung cancer (19), the most frequent tumor type in *Cbx7*-KO mice (see below). Therefore, we asked whether CBX7 could negatively regulate *CCNE1* expression and consequently modulate cell proliferation, thereby accounting for the increased cell growth rate of *Cbx7*-KO fibroblasts. First, we measured *Ccne1* expression in MEFs and tissues (kidney and lung) of $Cbx7^{+/+}$, $Cbx7^{+/-}$, and $Cbx7^{-/-}$ mice by qRT-PCR. As shown in Figure 3A, *Ccne1* expression levels were higher in *Cbx7*-KO MEFs and tissues than in the WT controls. Western blot analysis yielded the same results (Figure 2K and data not shown). Interestingly, restoration of *Cbx7* expression resulted in decreased *Ccne1* expression levels in $Cbx7^{-/-}$ MEFs, comparable to those observed in WT MEFs (Figure 3A). Moreover, *Ccne1* expression was reduced in MEFs derived from mice overexpressing *Cbx7* in a manner dependent on *Cbx7* level (Supplemental Figure 2A). Together, these results support the hypothesis that CBX7 negatively regulates *CCNE1*.

We next evaluated binding of the CBX7 protein to the *CCNE1* promoter in vitro by EMSA with an oligonucleotide spanning –51 to –12 bp upstream of the transcriptional starting site (TSS) of the human *CCNE1* promoter region, including an E2F-responsive element and an HMGA-responsive AT-rich stretch. Increasing amounts (5 and 20 ng) of the recombinant glutathione-S-transferase–CBX7 (GST-CBX7) protein bound to the ^{32}P-end-labeled double-strand oligonucleotide in a dose-dependent manner (Figure 3B, lanes 2 and 3). Binding specificity was demonstrated by competition experiments that showed loss of binding with the addition of a 400-fold molar excess of the specific unlabeled oligonucleotide (Figure 3B, lane 4). No binding was obtained when an oligonucleotide corresponding to a region of the *GAPDH* promoter was used as a negative control (Figure 3B, lanes 11 and 12).

To identify the region of CBX7 required for *CCNE1* promoter binding, we performed the same experiment with 2 recombinant mutated forms of the CBX7 protein: one containing only the

chromodomain (GST-CBX7-CHROMO) and another lacking the chromodomain (GST-CBX7-NO CHROMO). Only GST-CBX7-CHROMO specifically bound to the *CCNE1* promoter (Figure 3B, lanes 5–10), which indicates that the CBX7 protein is able to bind the *CCNE1* promoter in vitro through its chromodomain.

We next evaluated whether the CBX7 protein could bind to a human *CCNE1* promoter region, including the E-box, by performing ChIP assays. HEK 293 cells were transiently transfected with HA-tagged *CBX7* expression vector or empty vector. Cells were then crosslinked, and DNA-chromatin complexes were subjected to IP with anti-HA or IgG antibodies. The IP chromatin was subsequently analyzed by quantitative PCR (qPCR), using primers spanning the region of the human *CCNE1* promoter (–850 to –700 bp upstream of the TSS) covering an E-box region. As shown in Figure 3C, HA-tagged *CBX7* showed co-IP with the *CCNE1* promoter in cells transfected with *CBX7*. Moreover, CBX7 also bound to *CDH1* and *CDKN2A*, which have previously been identified as promoters (12, 20). Conversely, no amplification was observed with anti-IgG precipitates and when primers for the *GAPDH* promoter were used, indicative of the specificity of CBX7 binding to the *CCNE1* promoter.

The same results were obtained when we performed ChIP assays on $Cbx7^{+/+}$ and $Cbx7^{-/-}$ MEFs (Figure 3D) and lung tissues (Supplemental Figure 3), which also indicated that the endogenous CBX7 protein was able to bind the *CCNE1* promoter. Furthermore, the binding of Hdac2 to the *Ccne1* promoter was reduced in $Cbx7^{-/-}$ compared with $Cbx7^{+/+}$ cells (Figure 3E), which indicates that the presence of Cbx7 favors Hdac2 binding to the *Ccne1* promoter. Finally, to assess the functional consequences of CBX7 binding to the *CCNE1* promoter, we demonstrated that CBX7 dose-dependently reduced the transcriptional activity of the *CCNE1* promoter (Figure 3F).

HMGA1 displaces the HDAC2/CBX7 complex from the CCNE1 promoter. We previously demonstrated that the expression of HMGA proteins increases E2F activity by displacing HDACs from E2F-responsive promoters, including *CCNE1* (21). Therefore, we hypothesized that CBX7 influences *CCNE1* expression by interacting with HMGA1 and then antagonizing its activ-
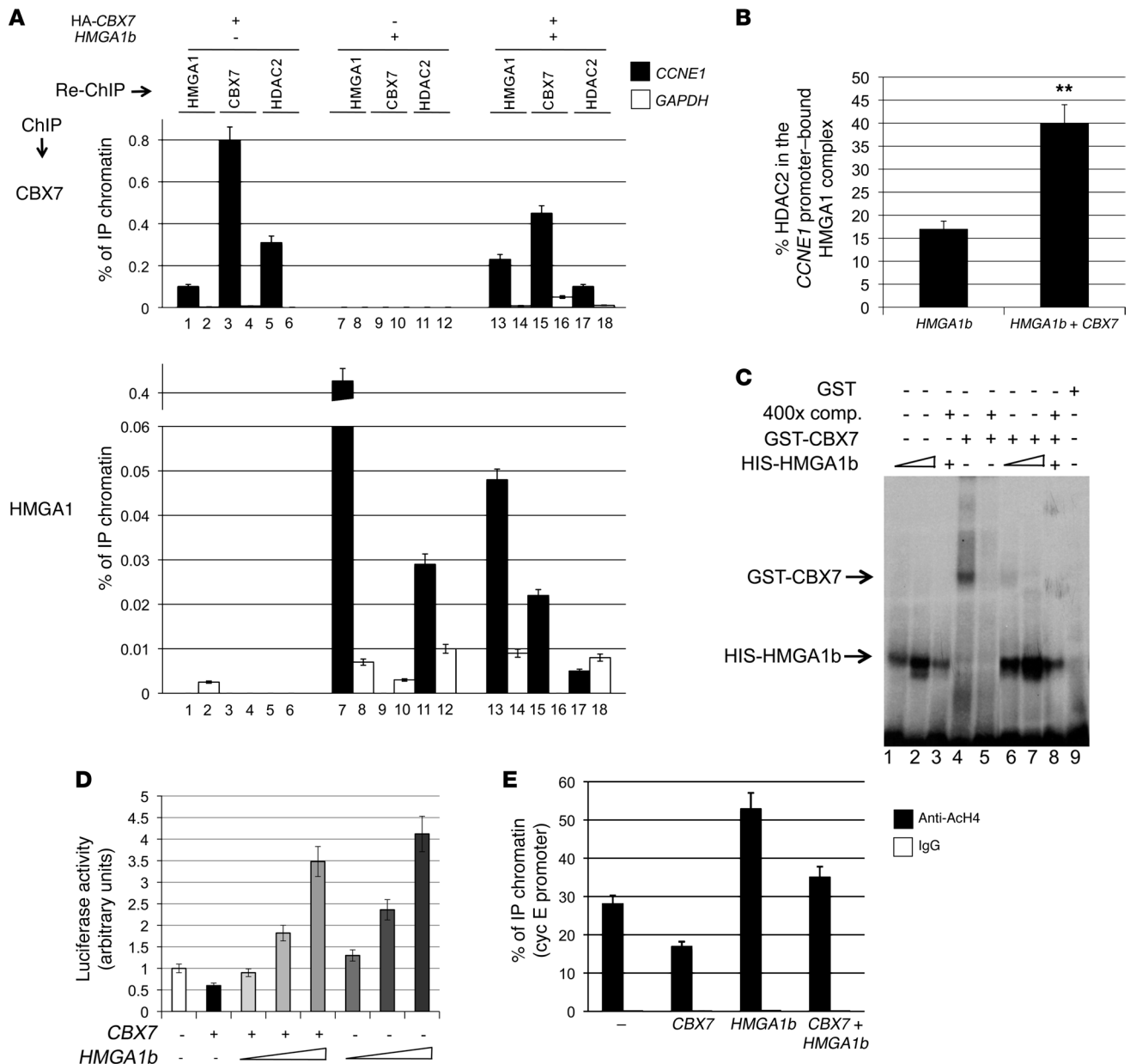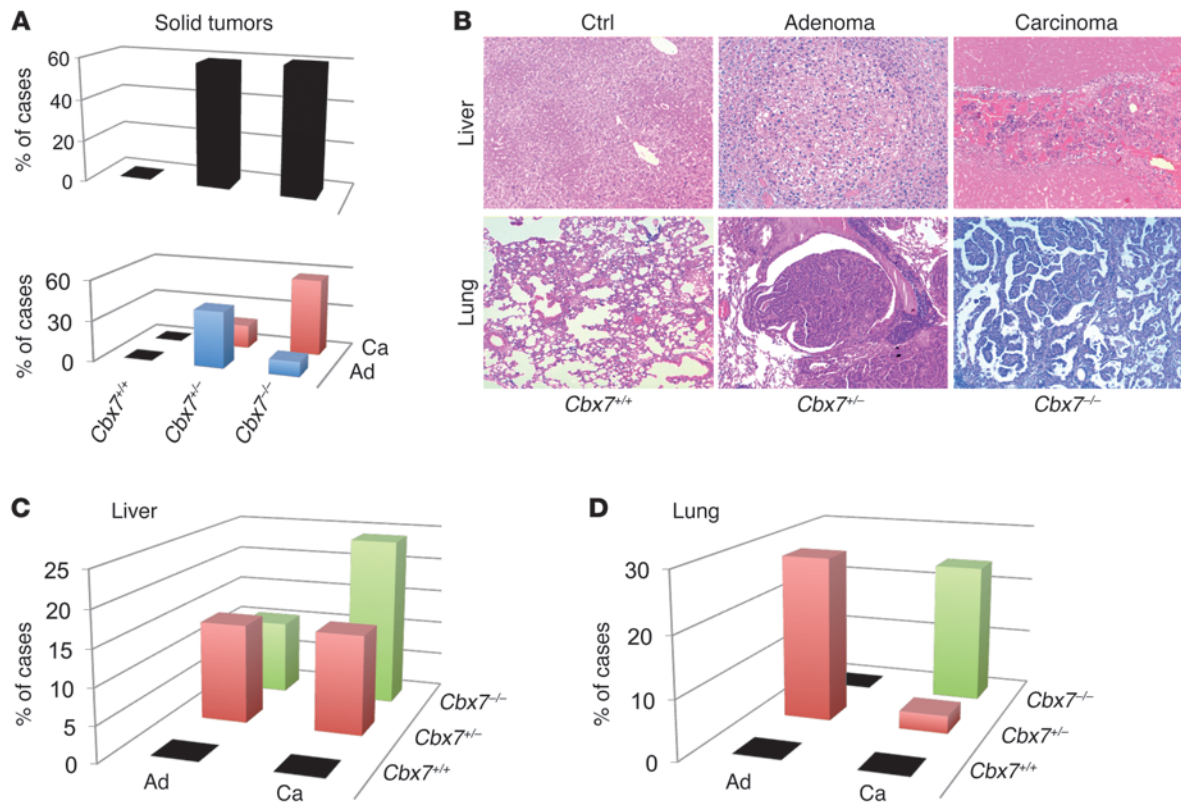
Figure 5
Competition between HMGA1 and CBX7 for binding, regulation, and acetylation of the *CCNE1* promoter. (**A**) ChIP and re-ChIP assay, revealed by qRT-PCR, on HEK 293 cells transfected with *HMGA1b* expression vector, HA-tagged *CBX7* expression vector, or both to detect the HMGA1/CBX7, CBX7/HDAC2, and HMGA1/HDAC2 interactions on the *CCNE1* promoter. *GAPDH* promoter was also analyzed as a negative control. (**B**) Percent HDAC2 protein co-IP with HMGA1, as detected in the ChIP and re-ChIP assay in **A**, comparatively reported in cells transfected with *HMGA1b* with or without *CBX7*. **$P < 0.01$. (**C**) EMSA, performed as in Figure 3B, using 5 ng GST-CBX7 (lanes 4–8) and 5 and 20 ng His-HMGA1b (lanes 1–3 and 6–8). A 400-fold molar excess of unlabeled probe (lanes 3, 5, and 8) was added as a specific competitor, and 5 ng of a recombinant GST protein (lane 9) was used as a negative control. (**D**) *CCNE1* promoter–driven luciferase activity, expressed relative to activation of empty vector–transfected cells, in HEK 293 cells. Where indicated, 1 μg *CBX7* and/or 1, 2, and 5 μg *HMGA1b* expression vectors were cotransfected with the cyclin E–luc plasmid. (**E**) ChIP assay, revealed by qRT-PCR, on HEK 293 cells transfected with *CBX7* expression vector, *HMGA1b* expression vector, both, or empty vector for binding of acetylated histone H4 (AcH4) to the *CCNE1* promoter. Equal amounts of proteins were subjected to IP with anti-AcH4 antibodies or nonspecific IgG, as indicated.

ity. To test this hypothesis, we transiently transfected HEK 293 cells with *CBX7* and *HMGA1b* expression constructs, subjected protein extracts to IP with anti-CBX7 or anti-HMGA1 antibodies, and immunoblotted them with the reciprocal antibodies. As shown in Figure 4A, coexpression of CBX7 and HMGA1b resulted

in reciprocal co-IP of the 2 proteins. Co-IP was performed in the presence of ethidium bromide to exclude that the co-IP of CBX7 and HMGA1b is dependent on contaminating DNA. The same result was obtained when co-IP was performed with the endogenous proteins extracted from WT mouse embryos (Figure 4B).

Figure 6
Cbx7-KO mice develop lung and liver tumors. (**A**) Frequency of spontaneous solid tumor development in 17- to 22-month-old mice of each geno-type (*n* = 11 [*Cbx7*+/+]; 34 [*Cbx7*+/−]; 24 [*Cbx7*−/−]). Ad, adenoma; Ca, carcinoma. (**B**) Representative liver and lung neoplasias in *Cbx7*-KO mice. Liver and lung tissues from *Cbx7*+/+ animals are shown on the left as normal controls. Original magnification, ×10. (**C** and **D**) Tumor incidence in livers (**C**) and lungs (**D**) from *Cbx7*+/+, *Cbx7*+/−, and *Cbx7*−/− mice.

Conversely, no interaction was detected when nonspecific IgGs were used (Figure 4, A and B). To verify this interaction, we carried out a pulldown assay using a GST-CBX7 recombinant protein; as shown in Figure 4C, GST-CBX7, but not GST, was able to pull down HMGA1b. Then, because of the ability of HMGA1b to inter-act with CBX7 (Figure 4) and of CBX7 to interact with HDAC2 (12), we investigated whether the physical interactions between CBX7 and either HDAC2 or HMGA1b take place on the *CCNE1* promoter. We performed ChIP and re-ChIP analysis on HEK 293 cells transiently transfected with HA-tagged *CBX7*, *HMGA1b*, or both expression vectors. Re-ChIP experiments were performed on exogenously expressed proteins because of the difficulty in obtaining good results when endogenous proteins are not highly expressed. The cells were crosslinked and subjected to IP with anti-HA antibodies recognizing the exogenous CBX7 protein. The CBX7 complexes were subjected to re-IP with anti-HMGA1, anti-HA, and anti-HDAC2 antibodies and then analyzed by qPCR for *CCNE1* promoter amplification using the same primers as above. The results demonstrated that CBX7, HMGA1b, and HDAC2 occupied the same region on the *CCNE1* promoter (Figure 5A, top). Moreover, HMGA1b expression led to a reduction of the CBX7/HDAC2 complex levels present at this promoter. The recip-rocal experiment, using anti-HDAC2 antibodies for the first ChIP, yielded comparable results (data not shown), whereas the ChIP for HMGA1 showed that CBX7 expression reduced the amount

of HMGA1 protein bound to the *CCNE1* promoter, suggestive of mutual competition between CBX7 and HMGA1 for the binding to this promoter. Interestingly, the amount of HDAC2 present in the *CCNE1* promoter–bound HMGA1b complex increased from 17% to 40% in the presence of CBX7 (Figure 5B). Taken together, these results indicate that CBX7 binds the *CCNE1* promoter and participates in the DNA-bound multimeric complex containing HDAC2 and HMGA1. These data also suggest that CBX7 recruits HDAC2 on the *CCNE1* promoter, whereas HMGA1 displaces the CBX7/HDAC2 complex from this promoter.

HMGA1 competes with CBX7 for binding and regulation of the CCNE1 promoter. To investigate possible functional interactions between HMGA1b and CBX7 on the *CCNE1* promoter, we first analyzed the in vitro binding of both proteins to this promoter by EMSA, using the GST-CBX7 protein with increasing amounts of a his-tidine-tagged HMGA1b (HIS-HMGA1b) recombinant protein. Both proteins specifically bound to the oligonucleotide used as probe (Figure 5C, lanes 1–5). Importantly, the GST-CBX7/DNA complex was dose-dependently inhibited by HIS-HMGA1b (Figure 5C, lanes 6 and 7), which confirmed the competition of these pro-teins for binding to the *CCNE1* promoter. Consistently, analysis of *CCNE1* promoter activity in the presence of CBX7 and increasing amounts of HMGA1b demonstrated that HMGA1b counteracted the negative activity of CBX7 on the *CCNE1* promoter (Figure 5D), thereby causing a switch from repression to activation.

Table 1

Neoplastic findings in *Cbx7*-KO mice

Pathology	Cbx7^{+/+}	Cbx7^{+/−}	Cbx7^{−/−}
Lymphoma	2/11 (18%)	6/34 (18%)	0/24 (0%)
Hepatocellular carcinoma	0/10 (0%)	4/29 (14%)	6/19 (32%)
Lung adenocarcinoma	0/9 (0%)	1/29 (3%)	5/21 (24%)
Lung adenoma	0/9 (0%)	8/29 (28%)	0/21 (0%)
Liver adenoma	0/10 (0%)	4/29 (14%)	2/19 (10.5%)

CBX7 expression results in increased histone acetylation of the CCNE1 promoter. Chromatin remodeling and histone modifications have recently emerged as the main mechanisms whereby gene expression is controlled. Since the link between DNA methylation and histone deacetylation in gene silencing is well established (22–26), we evaluated the lysine acetylation of histone tails at the *CCNE1* promoter. HEK 293 cells were transfected with V5-tagged *CBX7* expression vector (referred to herein as *CBX7-V5*) or with empty vector, cells were crosslinked, and DNA-chromatin was subjected to IP with anti–H4 acetylated or anti-IgG antibodies. IP chromatin was analyzed by qPCR with primers spanning the *CCNE1* promoter region. As shown in Figure 5E, the amounts of H4 acetylated tails were lower in the *CCNE1* promoter of CBX7-transfected cells than in backbone vector controls, which suggests that CBX7 decreases histone acetylation. No IP occurred with anti-IgG precipitates. Moreover, *CBX7* expression competed with the H4 acetylation–increasing activity of HMGA1b. Our data therefore suggest that CBX7 binds the *CCNE1* promoter and inhibits *CCNE1* transcription, counteracting the enhancement of *CCNE1* transcription by HMGA1b and modifying histone acetylation at its promoter.

Cbx7-KO mice develop liver and lung neoplasias. Neither *Cbx7^{−/−}* nor *Cbx7^{+/−}* mice showed any evidence of illness up to 12 months of age. Conversely, histopathological analysis revealed the presence of solid tumors in aged (17- to 22-month-old) *Cbx7^{+/−}* and *Cbx7^{−/−}* mice, but not in their *Cbx7^{+/+}* littermates (Figure 6A). These tumors included lung and liver neoplasias, ranging from adenoma to carcinoma (Figure 6B). In the case of liver neoplasias, an equal number of benign lesions was present in *Cbx7^{+/−}* and *Cbx7^{−/−}* mice, but there was a higher percentage of hepatocellular carcinomas in *Cbx7^{−/−}* than in *Cbx7^{+/−}* mice (32% vs. 14%; Table 1 and Figure 6C). Lung adenomas and adenocarcinomas occurred in *Cbx7^{+/−}* and *Cbx7^{−/−}* mice (28% and 24%, respectively); however, adenomas were detected only in *Cbx7^{+/−}* mice, whereas carcinomas were prevalent in *Cbx7^{−/−}* mice (Table 1 and Figure 6D). Immunohistochemical and qRT-PCR analyses of hepatocellular and lung carcinomas in *Cbx7^{−/−}* mice confirmed the absence of Cbx7 expression and showed cyclin E overexpression (data not shown). We assessed *Cdkn2a* and *Cdkn2d* levels qRT-PCR in the lung carcinoma samples and found increased *Cdkn2a* expression in the neoplastic tissues, in contrast to no clear differences in *Cdkn2d* expression observed between normal and carcinoma lung tissues (Supplemental Figure 4). This result is consistent with our previously published results showing that p16 is moderately overexpressed in papillary thyroid cancer (where CBX7 is moderately downregulated) and highly overexpressed in anaplastic thyroid cancer (where CBX7 is heavily downregulated) compared with normal thyroid tissues (6). The cellular context might play a critical role in the regulation of p16 by CBX7, and it is also likely that p16 is not effective in the neoplastic tissues: it might be just an attempt of the cells to contrast the proliferation signals.

CBX7 is drastically downregulated in human lung carcinomas. Because cyclin E overexpression plays a critical role in lung carcinogenesis (19, 27), we focused our attention on human lung tumors. We first evaluated CBX7 protein expression in a panel of human lung adenocarcinomas by immunohistochemistry. As shown in Table 2, CBX7 was not expressed in any of the lung carcinomas analyzed, whereas it was expressed in normal lung tissue. Moreover, analysis of *CBX7*- and *CCNE1*-specific mRNA expression by qRT-PCR revealed an inverse correlation between *CBX7* and *CCNE1* expression in lung carcinomas (Supplemental Figure 5).

Loss of heterozygosity (LOH) analysis at the *CBX7* locus revealed LOH in 50% of the informative carcinomas (Table 2). Interestingly, when the morphologically normal lung area adjacent to the tumor was analyzed for CBX7 expression, no staining occurred in 4 of 8 cases analyzed (Figure 7). In other cases, staining was weaker compared with the normal lung (data not shown). Moreover, the 4 samples negative for CBX7 expression showed LOH when we analyzed the DNA extracted from the same microdissected areas (Table 2), which suggests that the reduced CBX7 expression might be involved in the transition of lung cells to a completely transformed malignant stage.

Since, as shown above, CBX7 negatively regulates *CCNE1* promoter activity, we also evaluated cyclin E expression in the same lung neoplastic samples. In line with previous data (19, 27), cyclin E was overexpressed in all cases (Table 2 and Figure 7). Interestingly, cyclin E expression was higher in samples with LOH at the *CBX7* locus. Moreover, cyclin E was overexpressed in the areas adjacent to the lung carcinoma only when CBX7 expression was absent and LOH was detected at the *CBX7* locus (Table 2 and Figure 7).

To verify that CBX7 is a negative regulator of *CCNE1* expression in lung cells, we restored CBX7 expression in 2 lung carcinoma cell lines (A549 and H1299) that did not show any expression of CBX7 (Supplemental Figure 6A). Restoration of CBX7 expression resulted in a significant decrease in *CCNE1* expression, verified by qRT-PCR (Supplemental Figure 6B). Moreover, to further confirm that CBX7 downregulation could be a causative event in lung cell proliferation, we performed a colony-forming assay on the same lung carcinoma cell lines. As shown in Supplemental Figure 6C, the cells transfected with *CBX7* expression vector gave rise to a lower number of colonies compared with cells transfected with empty vector.

Discussion

Polycomb group proteins function as multiprotein complexes and are part of a gene regulatory mechanism that determines cell fate during normal and pathogenic development. They form transcriptional repressor modules that can be functionally divided into at

Table 2

CBX7 LOH and expression of CBX7 and cyclin E in lung normal and carcinoma tissues

Sample	LOH	CBX7 expression	Cyclin E expression
Normal lung	0/8	8/8	0/8
Lung carcinoma	5/10[A]	0/40	40/40[B]
Lung carcinoma adjacent tissues	4/8[A]	4/8[C]	4/8[C]

[A]Number of informative cases of 16 analyzed. [B]Lung carcinomas that did not show LOH had lower cyclin E expression than did other carcinoma samples. [C]Samples with LOH were negative for CBX7 expression and positive for cyclin E expression.
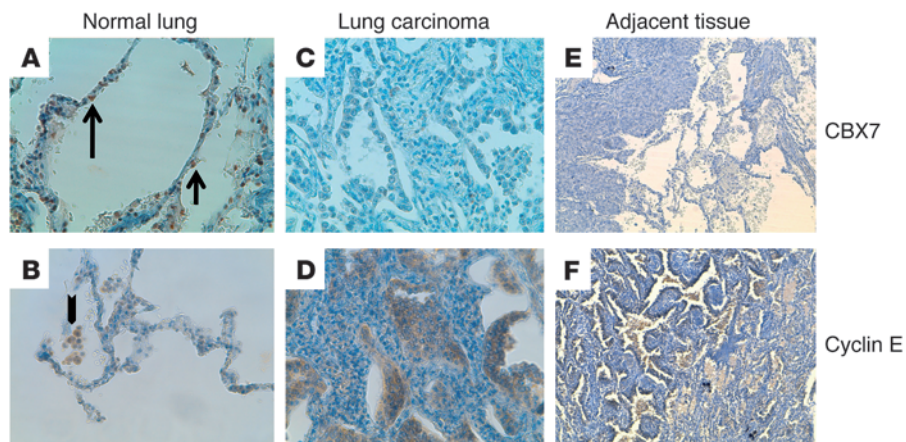
Figure 7
Immunohistochemical analysis of CBX7 and cyclin E expression in human normal and neoplastic lung tissues. (**A** and **B**) Normal lung had intense immunoreactivity for CBX7 (**A**, arrows), whereas it was negative for cyclin E expression (**B**). Arrowhead in **B** denotes positive histiocytes, a positive internal control. (**C** and **D**) Lung carcinoma was negative for CBX7 staining (**C**), but strongly positive for cyclin E expression (**D**). Higher-magnification views of **A**–**D** are provided in Supplemental Figure 7. (**E** and **F**) In a morphologically normal lung carcinoma–adjacent tissue, the tumoral part (top left) and the adjacent tissue (bottom right) did not express CBX7 (**E**), whereas both expressed high levels of cyclin E (**F**). Original magnification: ×63 (**A**–**D**); ×10 (**E** and **F**).

least 2 distinct complexes: (a) the initiation complex PRC2, the core of which in humans consists of EZH2, EED, and SUZ12; (b) the maintenance complex PRC1, whose components are the mammalian homologs of *Drosophila* polycomb (Pc), posterior sex combs (Psc), sex combs extra (Sce), and polyhomeiotic (Ph) proteins (28). CBX7 is a Pc homolog consisting of a conserved chromodomain near the N-terminus and a Pc box in the C-terminal region. Deregulation of PcG proteins contributes to tumorigenesis where aberrant silencing of PcG target genes is frequent (29). Indeed, EZH2 is amplified and highly expressed in many tumor types, and its expression correlates with high proliferation rate and poor outcome in breast, prostate, and other cancers (30, 31). Conversely, loss of CBX7 expression correlates with a highly malignant phenotype (6, 8, 9, 11, 12). The fact that EZH2 and CBX7 can physically associate with DNA methyltransferases (DNMTs) (32, 33) suggests a mechanism whereby PcG proteins directly contribute to the altered DNA methylation profiles that are observed in multiple cancer types. Indeed, PcG target genes are as much as 12 times more likely to be aberrantly silenced by DNA methylation in cancer than are non-PcG target genes (34–36). However, the role of CBX7 in the regulation of cell growth and tumorigenesis is still controversial, since there is also evidence that its overexpression leads to cellular immortalization in vitro and tumor development in vivo, thereby indicating that *CBX7* is an oncogene (3, 14). To address this issue, we generated and characterized *Cbx7*-KO mice.

The data reported here propose *CBX7* as a tumor suppressor gene. Consistent with our earlier finding that restoration of *CBX7* expression in thyroid carcinoma cells blocks the cells in G$_1$ phase (6), the proliferation rate of *Cbx7*-KO MEFs was higher than that of WT MEFs, and *Cbx7$^{-/-}$* mice developed neoplasias. However, in contrast to a report that CBX7 extends cellular lifespan (14), *Cbx7*-KO MEFs went to senescence later than did WT MEFs. This suggests that the cellular context plays a critical role in the effect of the CBX7 protein on cell growth. In the case of *Cbx7*-KO MEFs, the context may be considered more physiological than experiments in which CBX7 was ectopically overexpressed in HprECs and WI38 cells (14). It is possible

that *CBX7* overexpression deranges the composition of the PRC complexes, thereby causing unbalanced cell DNA methylation. Moreover, the same authors report reduced growth of both MEFs and human lung fibroblasts (WI38) when *CBX7* expression is silenced (14). The different experimental approach, ours in vivo and the previous one in vitro, may account for these contradictory results. Consistent with this hypothesis, it has been previously shown that in vivo data show significant discrepancies compared with in vitro data and transfection approaches when p53 pathway has been studied (37). Perhaps it is difficult to faithfully reproduce the relative ratios of CBX7 and its regulators and/or partners using transfection protocols. We also cannot exclude the hypothesis that the shRNA constructs used in the previous studies may have interfered with the expression of other genes, maybe of the Pc family. The behavior of MEFs derived from *Cbx7*-KO mice and Cbx7-overexpressing transgenic mice described herein is supported by the drastic downregulation of *CBX7* expression previously reported by several groups in malignant neoplasias — including thyroid (6), pancreatic (8), colon (11), lung (present study), gastric (10), bladder (7), and breast (9) carcinomas — and by a reduced growth rate achieved by restoration of CBX7 expression in carcinoma cells of different origin (6, 9, 11, 38).

The inhibition of *Ccne1* expression by Cbx7 seems to have a critical role in the phenotype of the *Cbx7*-KO mice. Indeed, *Ccne1* was expressed at higher levels in *Cbx7*-KO mice than in the WT controls, and CBX7 binds to the *CCNE1* promoter in a region that includes the E-box, thereby repressing its activity. The HMGA1b protein was a competitor of this action. The antagonistic effect of CBX7 versus HMGA1b protein on the *CCNE1* promoter, and perhaps other CBX7 target genes, probably accounts for most of the phenotypic features of the *Cbx7*-KO mice. Interestingly, HMGA and CBX7 act in an opposite manner in human malignancies: *HMGA* overexpression and *CBX7* downregulation correlate with a poor prognosis (6, 8, 11, 39, 40).

We also report that benign liver and lung adenomas were moderately frequent in *Cbx7$^{+/-}$* mice, whereas liver and lung carcinomas appeared in *Cbx7$^{-/-}$* mice, which suggests that the grade of malig-

nancy depends on the number of *Cbx7* functional alleles. To further probe the susceptibility of *Cbx7*-KO mice to neoplasias and evaluate the role of Cbx7 expression in cancer progression, we plan to cross these animals with transgenic mice carrying activated oncogenes and/or induce experimental neoplasias in *Cbx7*-KO mice.

Interestingly, all the human lung adenocarcinomas we analyzed showed the absence of *CBX7* expression, and LOH at the *CBX7* locus was frequent in these neoplasias. Interestingly, LOH at the *CBX7* locus also occurred in the morphologically normal tissue adjacent to lung tumor, in which CBX7 expression was significantly lower than in the normal lung tissues and cyclin E was overexpressed. These results suggest that the reduced CBX7 expression might facilitate the complete malignant lung cell transformation. Cyclin E overexpression in lung cells is probably the mechanism whereby loss of CBX7 expression contributes to lung carcinogenesis. Indeed, aberrant cyclin E expression is frequent in pulmonary dysplasia and lung cancer (19), and transgenic mice overexpressing cyclin E develop dysplasia and multiple pulmonary adenocarcinomas (41). However, in order to unequivocally demonstrate that cyclin E overexpression accounts for the phenotype of the *Cbx7*-KO mice, further experiments are required, specifically the generation of mice carrying the disruption of both *Cbx7* and *Ccne1* genes; the lack of development of lung carcinomas in these mice would validate our hypothesis.

In conclusion, our analysis of the phenotype of *Cbx7*-KO mice supports the concept that *CBX7* is a tumor suppressor gene, in seeming contrast with other published reports that *CBX7* behaves as an oncogene. It is conceivable that *CBX7* can exert both oncogenic and antioncogenic functions, depending on the nature of other cellular events and on the presence of interacting proteins. Moreover, beyond defining a tumor suppressor role of the *CBX7* gene, the data reported here indicate a critical role of the loss of *CBX7* expression in lung carcinogenesis as a likely precursor to *CCNE1* overexpression.

Methods

Generation and genotyping of mutant mice. For generation of KO mice, the *Cbx7* gene targeting vector was designed to delete the fifth and sixth codon of the mouse *Cbx7* gene. To clone the mouse *Cbx7* genomic locus, a λΦXII phage library of a 129SvJ mouse strain (Stratagene) was screened. The targeting vector was constructed by subcloning, in the Bluescript plasmid (Stratagene), the 5′-flanking region (*Bam*HI-*Dra*I 2.6 kb fragment), the *neo* cassette for positive selection, the 3′-flanking region (*Cla*I-*Bam*HI 2.3 kb fragment) and a TK gene cassette for negative selection. The targeting vector was linearized with *Not*I before electroporation into ES cells. 2 G418/ganciclovir-resistant ES clones were injected into C57BL/6J blastocysts, both of which gave rise to germline chimeras that were backcrossed to C57BL/6J females to obtain *Cbx7*+/− offspring. For Southern blot analysis, tail DNA samples were digested with *Eco*RI and probed with an external 5′ genomic fragment detecting 20-kb or 9-kb fragments corresponding to the WT and mutant alleles, respectively. *Cbx7*+/− mice were crossed with each other to yield *Cbx7*−/− animals.

For generation of transgenic mice, a 477-bp cDNA fragment corresponding to the entire coding sequence of the murine *Cbx7* gene was subcloned into the *Bam*HI and *Eco*RI sites of the expression vector pcDNA3.1/myc-His (−) B (Invitrogen). It was linearized with *Pvu*I and electroporated into ES 129SvJ cells. G418-resistant clones were selected and analyzed by PCR. 2 positive clones were microinjected into C57BL/6J mouse blastocysts and then transferred to pseudopregnant foster mothers. Chimeric mice were crossed to WT C57BL/6J mice, and germline

transmission of the transgene was checked by PCR analysis of tail DNA from agouti coat–colored F1 offspring. The primers used for the screening were as follows: forward, 5′-TAATACGACTCACTATAGGG-3′; reverse, 5′-TAGAAGGCACAGTCGAGG-3′.

All mice were maintained under standardized nonbarrier conditions in the Laboratory Animal Facility of Istituto dei Tumori di Napoli (Naples, Italy), and all studies were conducted in accordance with Italian regulations for experimentations on animals.

mRNA isolation, Northern blot analysis, and RT-PCR. Total RNA was extracted using TRI-reagent solution (Invitrogen) according to the manufacturer's protocol. Northern blot analysis was performed, as previously described (42), with 20 μg total RNA from *Cbx7*+/+ and *Cbx7*−/− tissue and cells. The probe was a 200-bp fragment covering the first 4 exons of the Cbx7 cDNA obtained by RT-PCR amplification, using forward and reverse *Cbx7* primers 5′-CATAGGCGAGCAGGTGTTTG-3′ and 5′-CTGGGTTTCG-GACCTCTCTT-3′, respectively, according to standard procedures (Applied Biosystems). qRT-PCR was performed with the SYBR Green PCR Master Mix (Applied Biosystems) under the following conditions: 10 minutes at 95°C, followed by 40 cycles (15 seconds at 95°C and 1 minute at 60°C). Each reaction was performed in duplicate. We used the $2^{-\Delta\Delta CT}$ method to calculate the relative expression levels (43). Details of primer sequences are provided in Supplemental Methods.

Growth and cell cycle analysis of MEFs. Primary MEFs were obtained from 12.5-day-old embryos. The MEFs were minced and used to establish single cell suspensions. They were grown in DMEM (Gibco; Invitrogen) containing 10% fetal bovine serum (Hyclone), 1% glutamine (Gibco; Invitrogen), 1% penicillin/streptomycin, and 1% gentamicin (Gibco; Invitrogen). The cells (4×10^5 cells/dish) were plated in a series of 6-cm culture dishes and counted daily with a hemocytometer for 13 consecutive days to extrapolate growth curves. Cell cycle analysis was performed as previously described (6) using a FACSCalibur cytofluorimeter (BD). For cell cycle analysis, MEFs in logarithmic growth were trypsinized, fixed in 70% ethanol, and stored at 4°C for a few days. Cells were then washed with PBS without Ca^{2+} and Mg^{2+}, stained with 50 μg/ml propidium iodide containing RNAse (20 μg/ml), and analyzed by FACS. Cell debris and fixation artifacts were gated out, and G_1, S, and G_2/M populations were quantified using CellQuest software (BD). A similar number of events was analyzed in each experiment.

SA–β-gal assay. 4×10^4 MEFs, plated 24 hours before the assay, were washed twice with PBS and immersed in fixation buffer (2% [w/v] formaldehyde, 0.2% [w/v] glutaraldehyde in PBS) for 7 minutes. After 3 additional PBS washes, the cells were allowed to stain overnight in staining solution (40 mM citric acid/sodium phosphate, pH 6.0; 150 mM NaCl; 2.0 mM $MgCl_2$; 1 mg/ml X-gal) at 37°C without CO_2 to avoid changes in pH. The next day, the staining solution was replaced with PBS, and the stained and unstained cells were counted by light microscopy (at least 24 fields).

Plasmids, transfections, and luciferase activity assays. Expression vectors encoding for *CBX7* (12), *HMGA1* (44), or the same amount of the empty vectors were transfected into HEK 293 cells growing in DMEM containing 10% FBS (Gibco; Invitrogen), 1% glutamine (Gibco; Invitrogen) and 1% penicillin/streptomycin (Gibco; Invitrogen), by calcium phosphate precipitation (45). Reporter construct (0.2 μg) was: pCycE-luc (donated by K. Helin, BRIC Biotech Research and Innovation Centre Copenhagen Biocenter, Copenhagen, Denmark). CMV–β-gal expression vector was used to normalize transfection efficiency according to galactosidase activity. Cells were harvested 36 hours after transfection, and lysates were analyzed for luciferase activities using the Dual Light kit (Tropix) and a luminometer (Lumat LB9507; Berthold). All assays were performed in duplicate in 3 independent experiments.

Cbx7-restored cell lines were obtained by reintroducing a Myc-His-tagged murine *Cbx7* in the *Cbx7*−/− MEFs using Neon Electroporation System (Invitrogen) according to the manufacturer's instructions.

EMSA. Protein/DNA binding was determined by EMSA as previously described (46). 5–20 ng of WT and mutant CBX7 recombinant protein (12) was incubated with radiolabeled oligonucleotide (specific activity, 8,000–20,000 cpm/fmol). The double-strand oligonucleotide used encompassed a region spanning base –51 to –12 of the human *CCNE1* promoter (5′-CCGGTTCCGCGCGCAGGGATTTTAAATGTCCCGCTCTGAG-3′). A radiolabeled oligonucleotide spanning –23 to +4 of the human *GAPDH* gene was used as a negative control.

ChIP and re-ChIP assays. Chromatin samples, derived from cells and tissue, were processed for ChIP and re-ChIP experiments as reported elsewhere (12). Samples were subjected to IP with the following specific antibodies: anti-HA (sc-805; Santa Cruz), anti-HDAC2 (05-814; Upstate), anti–acetyl H4 (06-866; Upstate), and anti-HMGA1 (44). For qPCR, 3 μl of 150 μl IP DNA was used with primers described below. *GAPDH* promoter amplicon was used as a negative control in all experiments. IgGs were used as nonspecific controls, and input DNA values were used to normalize the values from quantitative ChIP samples. Percent input was calculated as $2^{\Delta Ct} \times 3$, where ΔCt is the difference between Ct_{input} and $Ct_{cIP}20$. All quantitative ChIP data were derived from at least 3 independent experiments, and for each experiment, qPCR was performed in triplicate. Primer sequences are provided in Supplemental Methods.

Protein extraction, Western blotting, and co-IP. Protein extraction, Western blotting, and co-IP procedures were carried out as reported elsewhere (46). The antibodies used were as follows: anti-tubulin (sc-7649; Santa Cruz), anti-p21 (sc-397; Santa Cruz), anti-p19 anti-p16Ink4a (ab-54210; Abcam), anti–cyclin E (sc-481; Santa Cruz), anti-p53 (sc-126; Santa Cruz), anti–phospho-p53 (9284; Cell Signaling), anti–cyclin A (sc-751; Santa Cruz), anti-CBX7 (a primary antibody raised against the C-terminus of the human CBX7 protein; Neosystem), anti-CBX7 (sc-70232; Santa Cruz), anti-HA (sc-805; Santa Cruz), anti-V5 (Sigma-Aldrich), and anti-HMGA1 (44).

GST pulldown assay. Bacterial expressed GST and GST-HMGA1b proteins (45) were bound to glutathione agarose and used for binding assays with total extracts from HEK 293 cells transfected or not with CBX7-V5 expression plasmid. Briefly, proteins in the extracts were allowed to associate with the beads carrying either GST or GST-HMGA1b for 2 hours in NETN buffer (12) at 4°C. The protein complexes were washed 4 times in the same buffer, dissociated by boiling in loading buffer, and electrophoresed on a 12% polyacrylamide-SDS gel. The proteins were transferred to nitrocellulose, and CBX7-V5 was visualized as described above.

Histological and immnohistochemical procedures. Immunohistochemical analysis of CBX7 and cyclin E of paraffin-embedded tissues was performed, as previously described (6), using polyclonal antibodies raised against the C-terminal region of human CBX7 protein and commercial antibodies versus cyclin E (Santa Cruz), respectively. The specificity of the antibodies used was ascertained as previously described (6): no staining was observed when normal thyroid gland and lung samples were stained with antibodies pre-incubated with the peptide against which the antibodies were raised (6) or without the primary antibodies (data not shown).

LOH analysis. LOH analysis at the *Cbx7* locus on chromosome 22q13.1 was performed as previously described (6).

Colony-forming assay. Lung carcinoma cells (A549 and H1299), growing in RPMI containing 10% FCS (Gibco; Invitrogen), 1% glutamine (Gibco; Invitrogen), and 1% penicillin/streptomycin (Gibco; Invitrogen), were plated at a density of 90% in 100-mm dishes, transfected with 5 μg *CBX7*-HA expression vector or with the backbone vector, and supplemented with geneticin (G418) 24 hours later. 2 weeks after the onset of drug selection, cells were fixed and stained with crystal violet (0.1% crystal violet in 20% methanol).

Statistics. We used 2-tailed Student's *t* test for intergroup comparisons. A *P* value less than 0.05 was considered statistically significant.

Study approval. All animal procedures were reviewed and approved by the Institutional Ethical Committee at Centro Servizi Veterinari of the University of Naples "Federico II." Paraffin-embedded human lung cancer samples, with paired normal adjacent alveoli, were obtained from the Department of Scienze Biomorfologiche e Funzionali at the University of Naples "Federico II" under the guidelines of the IEOS review board. Informed consent was obtained from all patients for the scientific use of biological material.

Acknowledgments

Address correspondence to: Alfredo Fusco, Istituto di Endocrinologia ed Oncologia Sperimentale del CNR, Via Pansini 5, 80131 Naples, Italy. Phone: 39.081.7463602; Fax: 39.081.2296674; E-mail: afusco@napoli.com or alfusco@unina.it.

1. Schuettengruber B, Chourrout D, Vervoort M, Leblanc B, Cavalli G. Genome regulation by polycomb and trithorax proteins. *Cell*. 2007;128(4):735–745.
2. Wu JL, Lessard J, Crabtree GR. Understanding the words of chromatin regulation. *Cell*. 2009;136(2):200–206.
3. Scott CL, et al. Role of the chromobox protein CBX7 in lymphomagenesis. *Proc Natl Acad Sci U S A*. 2007;104(13):5389–5394.
4. Bernstein E, Duncan EM, Masui O, Gil J, Heard E, Allis CD. Mouse polycomb proteins bind differentially to methylated histone H3 and RNA and are enriched in facultative heterochromatin. *Mol Cell Biol*. 2006;26(7):2560–2569.
5. Lund AH, van Lohuizen M. Polycomb complexes and silencing mechanisms. *Curr Opin Cell Biol*. 2004;16(3):239–246.
6. Pallante P, et al. Loss of the CBX7 gene expression correlates with a highly malignant phenotype in thyroid cancer. *Cancer Res*. 2008;68(16):6770–6778.
7. Hinz S, et al. Expression of the polycomb group proteins BMI1, SUZ12, RING1 and CBX7 in urothelial carcinoma of the bladder and their prognostic relevance. *Tumour Biol*. 2008; 29(5):323–329.
8. Karamitopoulou E, et al. Loss of the CBX7 protein expression correlates with a more aggressive phenotype in pancreatic cancer. *Eur J Cancer*. 2010;46(8):1438–1444.
9. Mansueto G, et al. Identification of a new pathway for tumor progression: microRNA-181b up-regulation and CBX7 down-regulation by HMGA1 protein. *Genes Cancer*. 2010;1(3):210–224.
10. Jiang Z, et al. Increased expression of miR-421 in human gastric carcinoma and its clinical association. *J Gastroenterol*. 2010;45(1):17–23.
11. Pallante P, et al. The loss of the CBX7 gene expression represents an adverse prognostic marker for survival of colon carcinoma patients. *Eur J Cancer*. 2010;46(12):2304–2313.
12. Federico A, et al. Chromobox protein homologue 7 protein, with decreased expression in human carcinomas, positively regulates E-cadherin expression by interacting with the histone deacetylase 2 protein. *Cancer Res*. 2009;69(17):7079–7087.
13. Bernard D, et al. CBX7 controls the growth of normal and tumor-derived prostate cells by repressing the Ink4a/Arf locus. *Oncogene*. 2005;24(36):5543–5551.
14. Gil J, Bernard D, Martinez D, Beach D. Polycomb CBX7 has a unifying role in cellular lifespan. *Nat Cell Biol*. 2004;6(1):67–72.
15. Sherr CJ, DePinho RA. Cellular senescence: mitotic clock or culture shock? *Cell*. 2000;102(4):407–410.
16. Gray-Bablin J, Zalvide J, Fox MP, Knickerbocker CJ, DeCaprio JA, Keyomarsi K. Cyclin E, a redundant cyclin in breast cancer. *Proc Natl Acad Sci U S A*. 1996;93(26):15215–15220.
17. Kim S, et al. Histone deacetylase inhibitor apicidin induces cyclin E expression through Sp1 sites. *Biochem Biophys Res Commun*. 2006;342(4):1168–1173.
18. Leone G, et al. E2F3 activity is regulated during the cell cycle and is required for the induction of S phase. *Genes Dev*. 1998;12(14):2120–2130.
19. Lonardo F, Rusch V, Langenfeld J, Dmitrovsky E, Klimstra DS. Overexpression of cyclins D1 and E is frequent in bronchial preneoplasia and precedes squamous cell carcinoma development. *Cancer Res*. 1999;59(10):2470–2476.
20. Bracken AP, et al. The Polycomb group proteins bind throughout the INK4A-ARF locus and are disassociated in senescent cells. *Genes Dev*. 2007; 21(5):525–530.
21. Fedele M, et al. HMGA2 induces pituitary tumorigenesis by enhancing E2F1 activity. *Cancer Cell*. 2006;9(6):459–471.

22. Marks P, Rifkind RA, Richon VM, Breslow R, Miller T, Kelly WK. Histone deacetylases and cancer: causes and therapies. *Nat Rev Cancer*. 2001;1(3):194–202.

23. Bolden JE, Peart M, Johnstone RW. Anticancer activities of histone deacetylase inhibitors. *Nat Rev Drug Discov*. 2006;5(9):769–784.

24. Minucci S, Pelicci PG. Histone deacetylase inhibitors and the promise of epigenetic (and more) treatments for cancer. *Nat Rev Cancer*. 2006;6(1):38–51.

25. Smith CL. A shifting paradigm: histone deacetylases and transcriptional activation. *Bioessays*. 2008;30(1):15–24.

26. Kouzarides T. Chromatin modifications and their function. *Cell*. 2007;128(4):693–705.

27. Fukuse T, Hirata T, Naiki H, Hitomi S, Wada H. Prognostic significance of cyclin E overexpression in resected non-small cell lung cancer. *Cancer Res*. 2000;60(2):242–244.

28. Valk-Lingbeek ME, Bruggeman SW, van Lohuizen M. Stem cells and cancer; the polycomb connection. *Cell*. 2004;118(4):409–418.

29. Bracken AP, Helin K. Polycomb group proteins: navigators of lineage pathways led astray in cancer. *Nat Rev Cancer*. 2009;9(11):773–784.

30. Yu J, et al. Integrative genomics analysis reveals silencing of beta-adrenergic signalling by polycomb in prostate cancer. *Cancer Cell*. 2007;12(5):419–431.

31. Yu J, et al. A polycomb repression signature in metastatic prostate cancer predicts cancer outcome. *Cancer Res*. 2007;67(22):10657–10663.

32. Vire E, et al. The Polycomb group protein EZH2 directly controls DNA methylation. *Nature*. 2006; 439(7078):871–874.

33. Mohammad HP, et al. Polycomb CBX7 promotes initiation of heritable repression of genes frequently silenced with cancer-specific DNA hypermethylation. *Cancer Res*. 2009;69(15):6322–6330.

34. Ohm JE, Baylin S-B. Stem cell chromatin patterns: an instructive mechanism for DNA hypermethylation? *Cell Cycle*. 2007;6(9):1040–1043.

35. Schlesinger Y, et al. Polycomb-mediated methylation on Lys27 of histone H3 pre-marks genes for de novo methylation in cancer. *Nat Genet*. 2007; 39(2):232–236.

36. Widschwendter M, et al. Epigenetic stem cell signature in cancer *Nat Genet*. 2007;39(2):157–158.

37. Toledo F, Wahl GM. Regulating the p53 pathway: in vitro hypotheses, in vivo veritas. *Nat Rev Cancer*. 2006;6(12):909–923.

38. Li Q, et al. Polycomb CBX7 directly controls trimethylation of histone H3 at lysine 9 at the p16 locus. *PLoS One*. 2010;5(10):e13732.

39. Fusco A, Fedele M. Roles of HMGA proteins in cancer. *Nat Rev Cancer*. 2007;7(12):899–910.

40. Fedele M, Fusco A. HMGA and cancer. *Biochim Biophys Acta*. 2010;1799(1–2):48–54.

41. Ma Y, et al. Transgenic cyclin E triggers dysplasia and multiple pulmonary adenocarcinomas. *Proc Natl Acad Sci U S A*. 2007;104(10):4089–4094.

42. Sambrook J, Fritsch EF, Maniatis T. *Molecular Cloning: A Laboratory Manual*. 2nd ed. Cold Spring Harbor, New York, USA: Cold Spring Harbor Laboratory Press; 1989.

43. Livak KJ, Schmittgen TD. Analysis of relative gene expression data using real-time quantitative PCR and the 2(-Delta Delta C(T)) Method. *Methods*. 2001; 25(4):402–408.

44. Pierantoni GM, Rinaldo C, Esposito F, Mottolese M, Soddu S, Fusco A. High mobility group A1 (HMGA1) proteins interact with p53 and inhibit its apoptotic activity. *Cell Death Differ*. 2006;13(9):1554–1563.

45. Melillo RM, et al. Critical role of the HMGI(Y) proteins in adipocytic cell growth and differentiation. *Mol Cell Biol*. 2001;21(7):2485–2495.

46. Esposito F, Tornincasa M, Chieffi P, De Martino I, Pierantoni GM, Fusco A. High-mobility group A1 proteins regulate p53-mediated transcription of Bcl-2 gene. *Cancer Res*. 2010;70(13):5379–5388.